NASA Contractor Report 145278

RADAR BACKSCATTERING FROM A SEA HAVING AN ANISOTROPIC LARGE-SCALE SURFACE

FRANK J. WENTZ

FRANK J. WENTZ AND ASSOCIATES
Box 162, MIT P. O.
CAMBRIDGE, MA 02139

NASA PURCHASE ORDER L-24420A

National Aeronautics and Space Administration

Langley Research Center
Hampton, Virginia 23665

TABLE OF CONTENTS

INTRODUCTION AND SUMMARY

Radar backscattering from the sea is governed by two distinct physical processes. For viewing angles θ near nadir the backscattering is primarily specular reflections from sea waves with wavelengths much longer than the radiation wavelength λ. The geometric-optics formulation of this large-scale scattering results in the normalized radar cross section σ^o being proportional to the probability density function $P(\hat{n})$ of the large-scale surface normal $\hat{n}$. For large nadir viewing angles the backscattering is principally Bragg scattering from sea waves with wavelengths comparable to λ, and σ^o depends on the power spectrum $W(\vec{\kappa},\hat{n})$ of these small-scale waves. The argument $\vec{\kappa}$ denotes the vector sea wavenumber, and $\hat{n}$ denotes the normal of the underlying large-scale roughness.

In this report we derive a two-scale scattering model that combines the two types of scattering in a manner consistent with energy conservation, that includes the effect of the tilting of the small-scale roughness by the large-scale roughness, and that accounts for the reduction of reflected power due to Bragg scattering. The special case of backscattering for which the transmitted polarization equals the received polarization is then considered. An anisotropic large-scale surface of the type reported by Cox and Munk [1956] is used to specify $P(\hat{n})$. In order to isolate the azimuthal variation of σ^o produced by the anisotropic $P(\hat{n})$, we assume an isotropic small-scale spectrum.

Computations of σ^o are compared with the AAFE RADSCAT data at 13.9 GHz for three wind speeds, U = 3, 6.5, and 15 m/s. Better agreement occurs for small and large θ than for intermediate angles. The poor agreement in the midrange may be cause by the abrupt splitting of the sea spectrum into large- and small-scale components and by the somewhat arbitrary choice of 0.25 for the perturbation parameter. The 3 m/s data are considerably less than the computed values at large nadir angles, and this may be due to the friction velocity being less than the critical velocity required to significantly disturb the surface. At 15 m/s the model displays an anisotropy that closely corresponds to the measured data. The anisotropy of the model decreases with decreasing wind speed, and the 3 m/s computations are essentially independent of the azimuth viewing angle ϕ. In contrast, the anisotropy of the measurements does not change much with wind speed, and for light winds it is probably due to a directional small-scale spectr m, which is not considered in the present model.

Parametric computations of σ^o at 14.6 GHz are also presented. The skewness of $P(\hat{\eta})$ results in the ratio of the upwind to downwind σ^o being less than unity for small θ. This agrees with X-band measurements [Skolnik, 1970] except that the ratio for the measurements is smaller than that given by the model. The average $<\sigma^o>$ of the upwind, crosswind, and downwind σ^o is also found. For small θ, $<\sigma^o>$ decreases with increasing wind speed, and at large angles the opposite is true. The average is least sensitive to wind speed variations near 15^o. At 30^o the wind dependence is approximately U^2 for horizontal polarization and $U^{1.5}$ for vertical polarization when $U \leq 20$ m/s. For large angles the horizontally polarized $<\sigma^o>$ has a stronger wind dependence than does the vertically polarized $<\sigma^o>$. Finally, the dependence of $<\sigma^o>$ on θ and on polarization diminishes for strong winds.

TWO-SCALE SCATTERING MODEL

The mean sea surface defines the $z = 0$ plane of a x,y,z coordinate system, and the x axis points in the upwind direction. All vectors are referenced to this system. Unit vectors are denoted by a caret, and vectors that in general do not have unit magnitude are denoted by an arrow. The axis vectors are denoted by $\hat{x}$, $\hat{y}$, and $\hat{z}$. The components of a vector are indicated by deleting the caret or arrow and inserting the superscript x, y, or z. The radar boresight direction is represented by $\hat{k}_i$ pointing towards the sea surface Σ, and the viewing angle θ is defined as the angle made by $-\hat{k}_i$ and $\hat{z}$.

The definition of scattering coefficient, which will be used throughout this report, is the ratio of the power density $p(\hat{k}_s)$ to the time-averaged power incident onto the surface in question, where $p(\hat{k}_s)dk_s^x dk_s^y$ is the time-averaged scattered power having a propagation vector in the neighborhood $dk_s^x dk_s^y$ of $\hat{k}_s$. This is not the usual definition but is more compatible with the $\hat{k}_i,\hat{k}_s$ vector notation used herein. Note that the integral of the scattering coefficient over all $\hat{k}_s$ equals the ratio of the total scattered power to the incident power. The scattering coefficient defined by Peake [1959] is in terms of power scattered per solid angle and is found by multiplying our coefficient by $4\pi k_s^z$ (a differential solid angle $d\Omega = dk_s^x dk_s^y / k_s^z$). The normalized radar cross section $\sigma^o(\hat{k}_i)$ is given by the product of Peake's scattering coefficient and $\cos\theta$. Hence in terms of our scattering coefficient $\Gamma(\hat{k}_i,\hat{k}_s)$ for the sea surface, the normalized radar cross section is

$$\sigma^o(\hat{k}_i) = 4\pi \cos^2\theta \; \Gamma(\hat{k}_i,-\hat{k}_i) \tag{1}$$

A two-scale scattering model is used to compute $\Gamma(\hat{k}_i,\hat{k}_s)$. The sea surface is modeled by a small-scale surface Σ_s superimposed onto a large-scale surface Σ_ℓ. The two-scale surface Σ is then the sum of Σ_s and Σ_ℓ. The rms height variation on Σ_s is assumed small compared to the radiation wavelength λ, and the rms slope variation is assumed small compared to unity. These two requirements are necessary for the application of perturbation theory [Rice, 1951] in treating the radiation scattered by Σ_s. The radius of curvature R_c at all points on Σ_ℓ is assumed much greater than λ. This allows for dividing Σ_ℓ into finite surface elements $\Delta\Sigma_\ell$ that have dimensions large relative to λ and that are nearly flat in the respect that the variation of the normal to $\Delta\Sigma_\ell$ is small compared to the mean normal $\hat{n}$ of $\Delta\Sigma_\ell$. The electric field on the two-scale surface element $\Delta\Sigma$ associated with $\Delta\Sigma_\ell$ is approximated by the field that would be present on the infinte plane normal to $\hat{n}$, Σ_s being superimposed on the plane. Furthermore, the fields on adjacent elements are assumed uncorrelated. This results in the scattering coefficient of $\Delta\Sigma$ being equal to the scattering coefficient $\Gamma(\hat{k}_i,\hat{k}_s,\hat{n})$ of the tilted small-scale surface Σ_s, and the total scattered power is the sum of the power scattered by the individual elements. Multiple scattering is not considered, and all of the scattered power is assumed to escape from the surface.

The power density $p(\hat{k}_s)$ for the two-scale surface is found by summing over all surface elements that are illuminated by the incident radiation.

$$p(\hat{k}_s) = \sum_m \Gamma(\hat{k}_i,\hat{k}_s,\hat{n}_m)\ \Delta p_i(\hat{k}_i,\hat{n}_m) \tag{2}$$

where $\hat{n}_m$ is the mean normal for the m^{th} element and $\Delta p_i(\hat{k}_i,\hat{n}_m)$ is the power incident onto the m^{th} element. Dividing (2) by the total incident power gives the scattering coefficient for the two-scale surface.

$$\Gamma(\hat{k}_i,\hat{k}_s) = (A\cos\theta)^{-1}\sum_m \Gamma(\hat{k}_i,\hat{k}_s,\hat{n}_m)\ \Delta A_m\ (-\hat{k}_i\cdot\hat{n}_m) \tag{3}$$

where A is the area of the mean two-scale surface that is subtended by the incident plane wave and ΔA_m is the area of $\Delta\Sigma_\ell$ for the m^{th} element. The assumption that the dimension of $\Delta\Sigma_\ell$ is small relative to R_c means that the variation in $\hat{\eta}$ from one element to the next is small, and hence the above summation can be replaced by the integral

$$\Gamma(\hat{k}_i,\hat{k}_s) = (A \cos \theta)^{-1} \int d\eta^x \int d\eta^y \; (-\hat{k}_i \cdot \hat{\eta}) \; \xi(\hat{k}_i,\hat{\eta}) \; \Gamma(\hat{k}_i,\hat{k}_s,\hat{\eta}) \tag{4}$$

where $\xi(\hat{k}_i,\hat{\eta})d\eta^x d\eta^y$ is the area of Σ_ℓ that has a normal in the neighborhood $d\eta^x d\eta^y$ of $\hat{\eta}$ and that is illuminated by the incident radiation. The region of integration is $(\eta^x)^2 + (\eta^y)^2 \leq 1$.

Let $\Xi(\hat{\eta})d\eta^x d\eta^y$ denote the area of Σ_ℓ that has a normal in the neighborhood $d\eta^x d\eta^y$ of $\hat{\eta}$ and that is subtended by the incident wave. The probability density function $P(\hat{\eta})$ of the large-scale surface normal is then defined by

$$P(\hat{\eta}) = \eta^z \; \Xi(\hat{\eta})/A \tag{5}$$

Let $I(\hat{k}_i,\hat{\eta})$ be the fraction of $\Xi(\hat{\eta})d\eta^x d\eta^y$ that is not shadowed by a remote portion of the surface from the incident radiation. The illuminated area density function $\xi(\hat{k}_i,\hat{\eta})$ is then given by the product of $\Xi(\hat{\eta})$ and $I(\hat{k}_i,\hat{\eta})$.

$$\xi(\hat{k}_i,\hat{\eta}) = I(\hat{k}_i,\hat{\eta}) \; P(\hat{\eta}) \; A/\eta^z \tag{6}$$

The illumination function $I(\hat{k}_i,\hat{\eta})$ is readily found by assuming that it is independent of $\hat{\eta}$ except through the unit step function $u(-\hat{k}_i \cdot \hat{\eta})$, which accounts for the situation in which the angle between $\hat{\eta}$ and $-\hat{k}_i$ exceeds $\pi/2$, totally ruling out the possibility of illumination.

$$I(\hat{k}_i,\hat{\eta}) = \chi(\hat{k}_i) \; u(-\hat{k}_i \cdot \hat{\eta}) \tag{7}$$

The function $\chi(\hat{k}_i)$ is determined as follows. The ratio of the power incident onto area $\xi(\hat{k}_i,\hat{\eta})d\eta^x d\eta^y$ to the total incident power is given by

$$r(\hat{k}_i,\hat{\eta}) = (A \cos \theta)^{-1} \; (-\hat{k}_i \cdot \hat{\eta}) \; \xi(\hat{k}_i,\hat{\eta})d\eta^x d\eta^y \tag{8}$$

The integral of $r(\hat{k}_i,\hat{n})$ over all $\hat{n}$ is unity, and solving for $\chi(\hat{k}_i)$ one obtains

$$\chi(\hat{k}_i) = \cos\theta \Big/ \int d\eta^x \int d\eta^y \, G(\hat{k}_i,\hat{n}) \tag{9}$$

$$G(\hat{k}_i,\hat{n}) = (-\hat{k}_i\cdot\hat{n}) \, u(-\hat{k}_i\cdot\hat{n}) \, P(\hat{n})/n^z \tag{10}$$

For situations in which shadowing is insignificant, such as smooth seas or small θ, $\chi(\hat{k}_i)$ approaches unity. Substituting (6) and (7) into (4) yields

$$\Gamma(\hat{k}_i,\hat{k}_s) = \chi(\hat{k}_i) \sec\theta \int d\eta^x \int d\eta^y \, G(\hat{k}_i,\hat{n}) \, \Gamma(\hat{k}_i,\hat{k}_s,\hat{n}) \tag{11}$$

In the Appendix $\Gamma(\hat{k}_i,\hat{k}_s,\hat{n})$ is derived as the sum of two scattering coefficients, one associated with the incoherent scattered power and the other with the coherent reflected power. The coherent coefficient given by (A25) has the form of a Dirac delta function, and when it is substituted into (11) yields

$$\Gamma_o(\hat{k}_i,\hat{k}_s) = \chi(\hat{k}_i) \sec\theta \, P(\hat{n}_o) \, \gamma(\hat{k}_i,\hat{n}_o)/4k_s^z \tag{12}$$

$$\hat{n}_o = (\hat{k}_s - \hat{k}_i)/|\hat{k}_s - \hat{k}_i| \tag{13}$$

where the power reflection coefficient $\gamma(\hat{k}_i,\hat{n}_o)$ is given by (A24).

We now consider the special case of backscattering, i.e., $\hat{k}_s = -\hat{k}_i$, for which the transmitted polarization equals the received polarization. Also the roughness on the small-scale surface Σ_s is assumed isotropic. Under these conditions (12) becomes

$$\Gamma_o(\hat{k}_i,-\hat{k}_i) = \tfrac{1}{4} \, \chi(\hat{k}_i) \sec^2\theta \, P(-\hat{k}_i) \, \gamma(\hat{k}_i,-\hat{k}_i) \tag{14}$$

where $\gamma(\hat{k}_i,-\hat{k}_i)$ is given by (A32). The incoherent two-scale backscattering coefficient is given by

$$\Gamma_x(\hat{k}_i,-\hat{k}_i) = \chi(\hat{k}_i) \sec\theta \int d\eta^x \int d\eta^y \, G(\hat{k}_i,\hat{n}) \, \Gamma_x(\hat{k}_i,-\hat{k}_i,\hat{n}) \tag{15}$$

where $\Gamma_x(\hat{k}_i,-\hat{k}_i,\hat{n})$ is given by (A31). Summing the coherent and incoherent coefficients gives the two-scale backscattering coefficient.

$$\Gamma(\hat{k}_i,-\hat{k}_i) = \Gamma_o(\hat{k}_i,-\hat{k}_i) + \Gamma_x(\hat{k}_i,-\hat{k}_i) \tag{16}$$

SPECIFICATION OF SEA SURFACE ROUGHNESS

The two-scale scattering model requires as inputs two distributions that characterize the sea surface roughness. These are the small-scale roughness power spectrum $W(\vec{\kappa})$, $\vec{\kappa}$ being the vector wavenumber, and the probability density function $P(\hat{n})$ of the large-scale surface normal $\hat{n}$. For the purpose of isolating the effect of an anisotropic large-scale surface, we assume an isotropic small-scale spectrum $W(\kappa)$ that depends only on $\kappa = |\vec{\kappa}|$. Pierson and Stacy's [1973] empirical sea spectrum $S(\kappa)$ (Eqs. 2.5 - 2.9 in their report) is used to specify $W(\kappa)$. The amplitude of $S(\kappa)$ is a function of the friction velocity u_*, which in turn is a function of the wind speed, anemometer height, and air-sea temperature difference [Cardone, 1969].

The spectrum $S(\kappa)$ is divided into a large-scale spectrum $S_\ell(\kappa)$ and a small-scale spectrum $S_s(\kappa)$.

$$S_\ell(\kappa) = \begin{cases} S(\kappa) & \kappa \leq \kappa_c \\ 0 & \kappa > \kappa_c \end{cases} \tag{17}$$

$$S_s(\kappa) = \begin{cases} 0 & \kappa \leq \kappa_c \\ S(\kappa) & \kappa > \kappa_c \end{cases} \tag{18}$$

and $W(\kappa)$ is related to $S_s(\kappa)$ by

$$W(\kappa) = (2/\pi)\ S_s(\kappa)/\kappa \tag{19}$$

The value of the cutoff wavenumber κ_c is found by assigning a value to the small-scale perturbation parameter $k\zeta$, where k is the radiation wavenumber and ζ is the rms height variation on the small-scale surface. Integrating over the small-scale spectrum gives ζ^2.

$$\zeta^2 = (\pi/2) \int_0^\infty d\kappa\ \kappa\ W(\kappa) \tag{20}$$

or in terms of $S(\kappa)$

$$\zeta^2 = \int_{\kappa_c}^{\infty} d\kappa \; S(\kappa) \tag{21}$$

The above integral can be evaluated in closed form, ζ being expressed as a function of κ_c and u_*. The inverse of this function gives κ_c in terms of ζ and u_*. Perturbation theory requires that $k\zeta$ be small in comparison to unity, and setting $k\zeta$ equal to zero results in the two-scale model degenerating to geometric optics. We use an intermediate value of 0.25 for the radar cross section computations, and the values of κ_c appear in the next section.

The specification of the large-scale slope density $P(\hat{n})$ is based on Cox and Munk's [1956] measurements of the sun glitter on rough seas. Their data were reduced in terms of the probability density function $P(Z_u,Z_c)$ of the up/downwind and crosswind surface slopes, Z_u and Z_c. The relationship between $P(\hat{n})$ and $P(Z_u,Z_c)$ is

$$P(\hat{n}) = (n^z)^{-4} \; P(Z_u,Z_c) \tag{22}$$

$$Z_u = -n^x/n^z \tag{23}$$

$$Z_c = -n^y/n^z \tag{24}$$

where $(n^z)^4$ is the Jacobian relating the Z_u,Z_c coordinates to the n^x,n^y coordinates.

The sun glitter data were fitted to a two-dimensional Gram-Charlier series, and $P(Z_u,Z_c)$ was found to be close to Gaussian with some up/downwind skewness that increased with wind speed. The most probable slope for high winds was about $Z_u = -\tan 3^o$. The data also showed a peakedness, barely above the experimental error, such that the probability of very large and very small slopes was greater than Gaussian. These properties are explicated in the following expressions given by Cox and Munk:

$$P(Z_u,Z_c) = [1 + T(\mu,\nu)] \exp[-\tfrac{1}{2}(\mu^2 + \nu^2)]/(2\pi\langle Z_u^2\rangle^{\frac{1}{2}} \langle Z_c^2\rangle^{\frac{1}{2}}) \quad (25)$$

$$T(\mu,\nu) = c_1\mu(\nu^2-1) + c_2(\mu^3-3\mu) + c_3(\nu^4-6\nu^2+3) + c_4(\nu^2-1)(\mu^2-1) + c_5(\mu^4-6\mu^2+3) \quad (26)$$

$$\mu = Z_u/\langle Z_u^2\rangle^{\frac{1}{2}} \quad (27)$$

$$\nu = Z_c/\langle Z_c^2\rangle^{\frac{1}{2}} \quad (28)$$

where $\langle Z_u^2\rangle$ and $\langle Z_c^2\rangle$ are the up/downwind and crosswind slope variances. The skewness coefficients are functions of the wind speed U (in m/s)

$$c_1 = -(0.01 - 0.0086U)/2 \quad (29)$$

$$c_2 = -(0.04 - 0.033U)/6 \quad (30)$$

and the peakedness coefficients are constants.

$$c_3 = 0.40/24 \quad (31)$$

$$c_4 = 0.12/4 \quad (32)$$

$$c_5 = 0.23/24 \quad (33)$$

The sun glitter from large and infrequent slopes was masked by a background of sunlight scattered by submerged particles and reflected skylight, and the values for the slope variances reported by Cox and Munk represent a lower bound [Wentz, 1975]. To correct for this and to filter out the slope contribution of the small-scale roughness, we multiply the Cox-Munk up/downwind and crosswind variances by the ratio of the total variance calculated from the Pierson-Stacy large-scale spectrum to the Cox-Munk total variance. The variances that are used in (25) are then

$$\langle Z_u^2 \rangle = (\langle Z^2 \rangle_{p-s} / \langle Z^2 \rangle_{c-m}) \langle Z_u^2 \rangle_{c-m} \tag{34}$$

$$\langle Z_c^2 \rangle = (\langle Z^2 \rangle_{p-s} / \langle Z^2 \rangle_{c-m}) \langle Z_c^2 \rangle_{c-m} \tag{35}$$

where the values of the variances reported by Cox and Munk are

$$\langle Z_u^2 \rangle_{c-m} = 3.16 \times 10^{-3} U \tag{36}$$

$$\langle Z_c^2 \rangle_{c-m} = 0.003 + 1.92 \times 10^{-3} U \tag{37}$$

and the total variance is

$$\langle Z^2 \rangle_{c-m} = \langle Z_u^2 \rangle_{c-m} + \langle Z_c^2 \rangle_{c-m} \tag{38}$$

The Pierson-Stacy total variance is calculated from

$$\langle Z^2 \rangle_{p-s} = \int_0^{\kappa_c} d\kappa \, \kappa^2 \, S(\kappa) \tag{39}$$

Although in the strictest sense (39) only applies to a Gaussian surface, the deviation from Gaussian indicated by the skewness and peakedness is slight and probably does not cause significant error in the variance calculation. Note that the Pierson-Stacy variances for the entire sea spectrum (found by integrating from 0 to ∞) are about twice as large as the Cox-Munk variances. The values of the total variances used in the radar cross section computations (i.e. the sum of (34) and (35), which equals $\langle Z^2 \rangle_{p-s}$) appear in the next section. The error in skewness and peakedness due to the lack of sun glitter data for large slopes is not considered.

COMPUTATIONS OF THE NORMALIZED RADAR CROSS SECTION

The backscattering model described in the previous two sections requires the following inputs: (1) radiation frequency f, (2) permittivity ϵ of seawater, (3) wind speed U, (4) nadir viewing angle θ, and (5) azimuth viewing angle ϕ. Two frequencies are considered: 13.9 GHz for the comparisons with the AAFE RADSCAT data and 14.6 GHz for the parametric computations. The permittivities for these two frequencies are shown in Tables 1 and 2 and are calculated from expressions given by Porter and Wentz [1971] for a seawater temperature and salinity of 284°K and 33 °/oo.

The sea surface roughness distributions $W(\kappa)$ and $P(\hat{n})$ discussed in the previous section depend on the wind speed U and friction velocity u_*. Cardone's [1969] expressions for a neutrally stratified atmosphere and for an anemometer height of 19.5 meters are used to calculate u_* as a function of U. Values for u_* along with the cutoff wavenumber κ_c and the large-scale slope variance $\langle Z^2 \rangle$, which are referred to in the preceding section, also appear in Tables 1 and 2.

Table 1. Inputs for the AAFE RADSCAT Comparisons

Frequency = 13.9 GHz

Permittivity = 40.1 - 39.3i

Wind Speed U (m/s)	Friction Velocity u_* (cm/s)	Cutoff Wavenumber κ_c (cm^{-1})	Slope Variance $\langle Z^2 \rangle$
3.0	10.4	0.79	0.018
6.5	21.5	0.97	0.032
15.0	61.9	1.63	0.097

Table 2. Inputs for the Parametric Computations

Frequency = 14.6 GHz

Permittivity = 38.4 - 39.0i

Wind Speed U (m/s)	Friction Velocity u_* (cm/s)	Cutoff Wavenumber κ_c (cm^{-1})	Slope Variance $\langle Z^2 \rangle$
5	16.0	0.93	0.026
10	37.2	1.27	0.054
15	61.9	1.71	0.099
20	91.1	2.28	0.175
25	122.4	2.93	0.293
30	158.5	3.75	0.492

The azimuth viewing angle ϕ is the angle made by the x axis, which points upwind, and the projection of the boresight vector $\hat{k}_i$ onto the z = 0 plane, which is the mean sea surface. The boresight direction is then specified by

$$\hat{k}_i = (\cos\phi \sin\theta, \sin\phi \sin\theta, -\cos\theta) \tag{40}$$

and $\phi = 0^\circ$, 90°, and 180° refer to measurements looking upwind, crosswind, and downwind, respectively. The backscattering model has no crosswind asymmetry, and hence the computations for ϕ and $-\phi$ are identical. The incident polarization vector $\hat{P}_i$, which appears in the Appendix, is calculated from

$$\hat{P}_i = \begin{cases} \hat{k}_i \times \hat{z} / |\hat{k}_i \times \hat{z}| & \text{horizontal polarization} \\ \hat{k}_i \times (\hat{k}_i \times \hat{z}) / |\hat{k}_i \times \hat{z}| & \text{vertical polarization} \end{cases} \tag{41}$$

Computations are done for the following directions:

$\theta = 0^\circ, 5^\circ, 10^\circ, 15^\circ, 20^\circ, 25^\circ, 30^\circ, 40^\circ, 50^\circ, 60^\circ$

$\phi = 0^\circ, 90^\circ, 180^\circ$

In addition, computations for 13.9 GHz and for $\theta = 30^\circ$ are done for ϕ ranging from 0° to 180° in 10° steps. In the figures these computation points are connected by straight lines.

The model is compared with the AAFE RADSCAT data at 13.9 GHz in Figures 1 through 5. The horizontally polarized normalized radar cross section σ_h^o is plotted versus the nadir viewing angle θ in Figures 1 through 3 for upwind, crosswind, and downwind observations. The short-dashed, long-dashed, and solid curves represent the computations for 3, 6.5, and 15 m/s winds, respectively. The measurements for these three wind speeds are indicated by squares, circles, and stars, respectively. The agreement between the model and the measurements is better for small and large values of θ than for intermediate values. At small nadir angles the backscattering is primarily specular reflections from the large-scale surface, whereas at large angles small-scale Bragg scattering dominates. The poor agreement in the transitional region may be due to the abrupt splitting of the sea spectrum into large- and small-scale components and to the somewhat arbitrary choice of 0.25 for the perturbation parameter.

The model displays a stronger wind dependence near nadir than do the measurements. At large angles, for which the opposite is true, the agreement at 15 m/s is fair, but the 3.5 m/s measurements are considerably less than the computations. Experiments in wind-water tunnels show a sudden increase in wave height at a critical friction velocity near 12 cm/s [Pierson and Stacy, 1973], and the expressions that are used to specify the sea spectrum are valid only for u_* greater than this critical velocity. The low values of the 3.5 m/s data at large angles possibly indicate that the friction velocity during these measurements was less than the critical velocity. This possibility is supported by the u_* calculations, which give a value of 10.4 cm/s for a 3.5 m/s wind speed.

In Figures 4 and 5, σ^o at $\theta = 30^{\circ}$ is plotted versus the azimuth viewing angle ϕ for horizontal and vertical polarizations. The same convention as

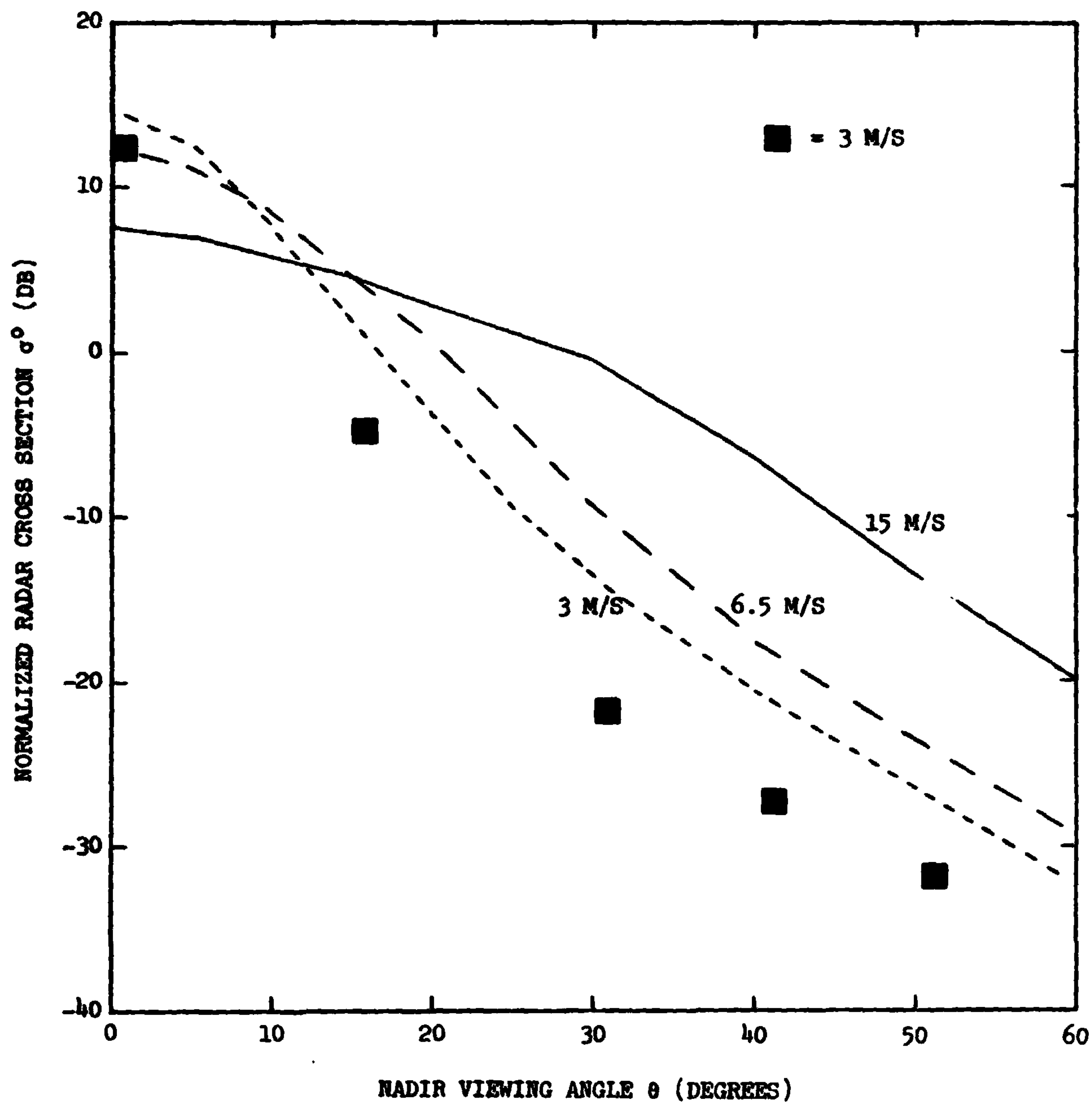

Fig. 1. Upwind normalized radar cross section for horizontal polarization

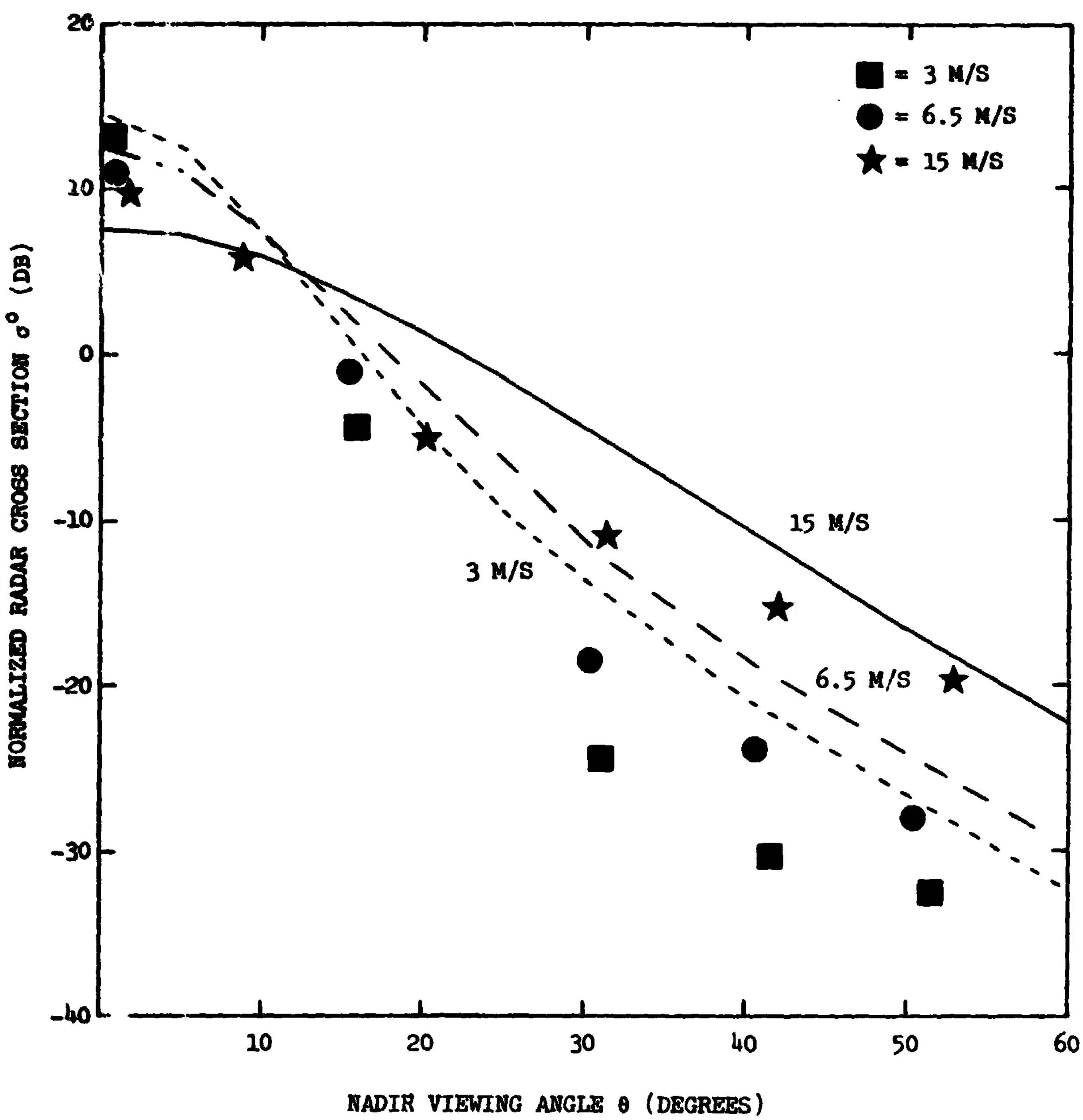

Fig. 2 Crosswind normalized radar cross section for horizontal polarization

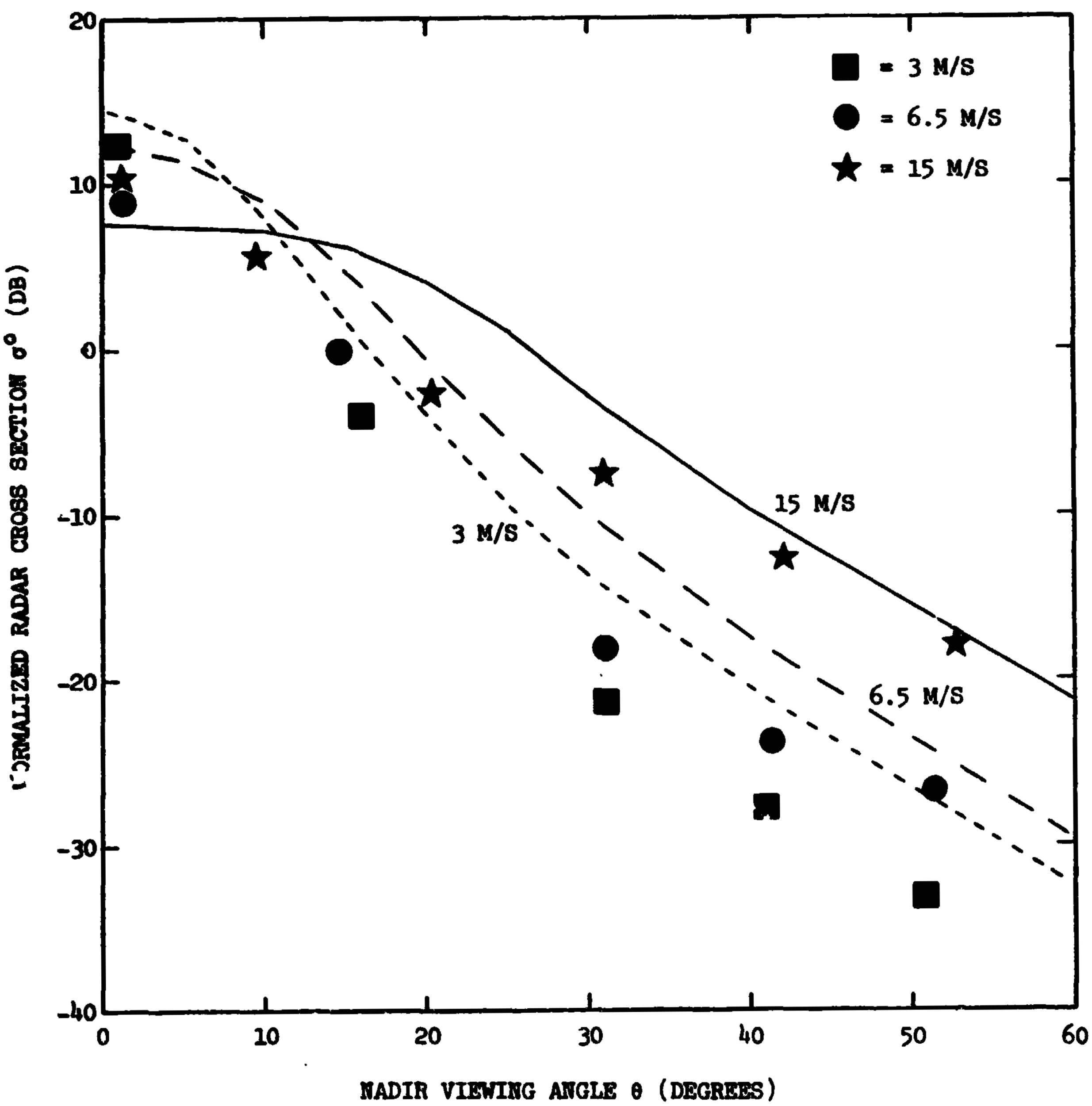

Fig. 3. Downwind normalized radar cross section for horizontal polarization

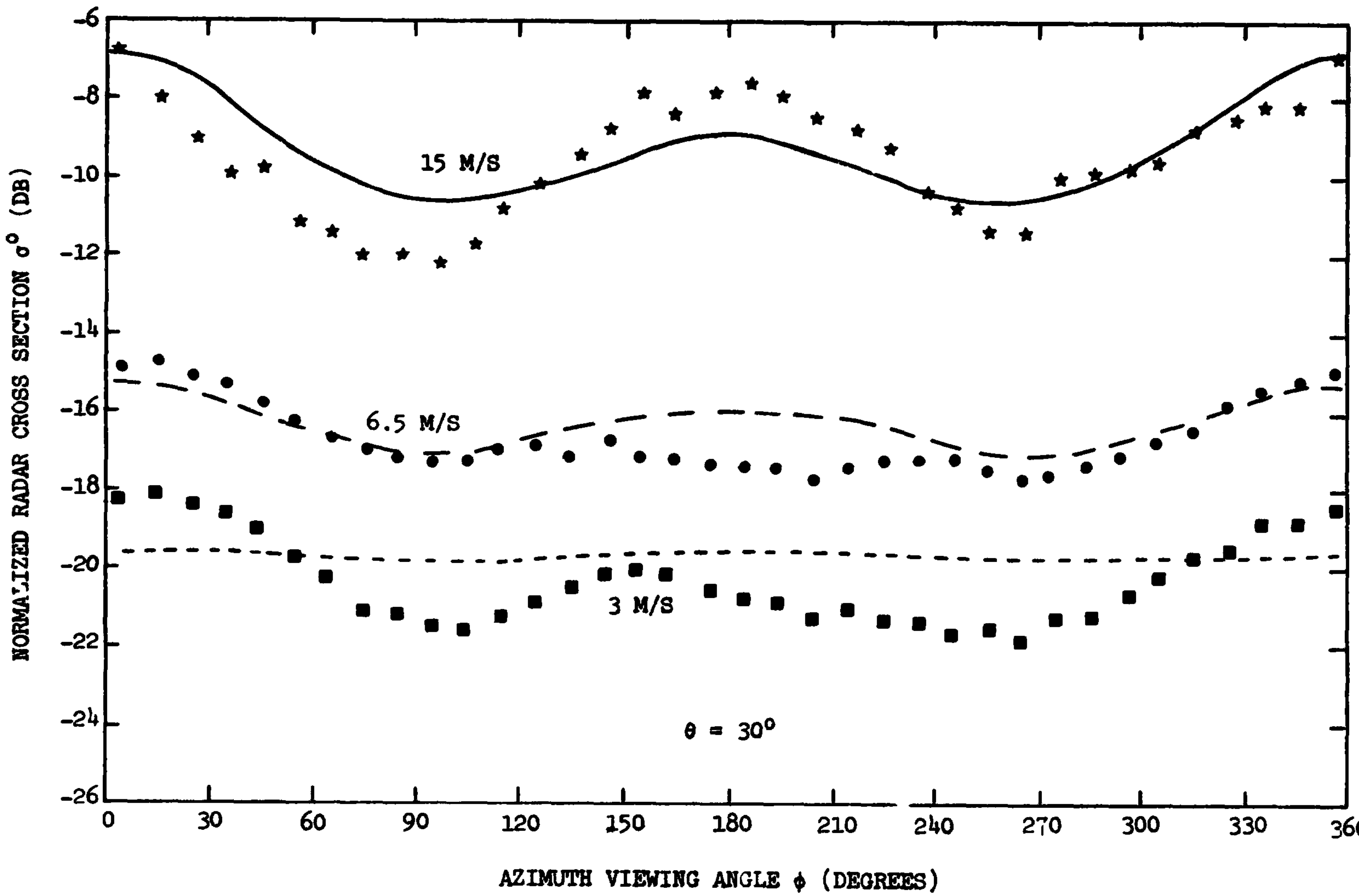

Fig. 4. Azimuth variation of the normalized radar cross section for horizontal polarization

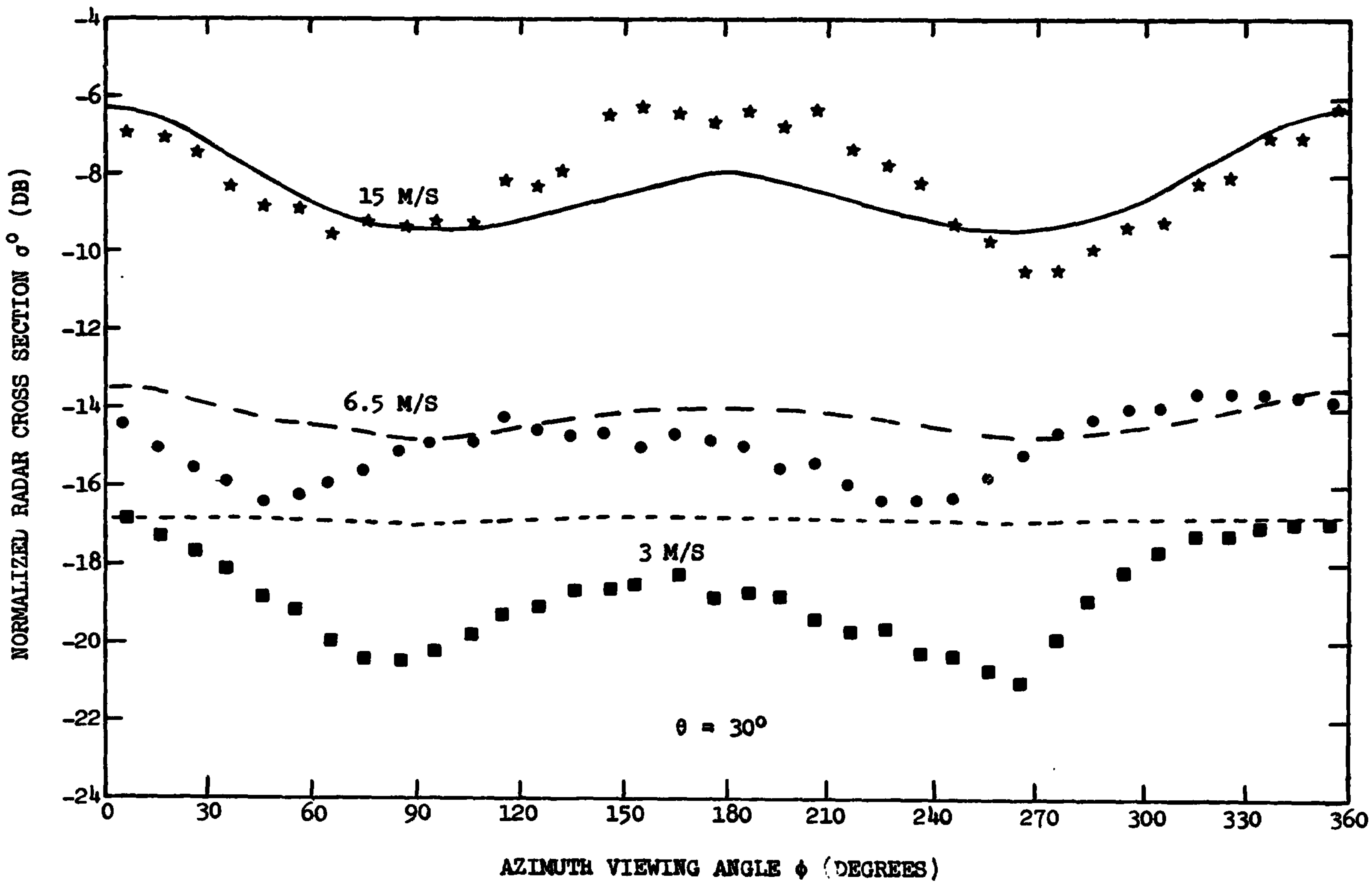

Fig. 5. Azimuth variation of the normalized radar cross section for vertical polarization

described above is used to identify the computations and measurements at the three wind speeds. A blanket 6 db has been subtracted from all computations in order to align them with the measurements. The spacing between the three wind speed curves agrees well with the observations. The 15 m/s curve shows a significant anisotropy that closely corresponds to the measured data. This dependence of the model on ϕ is due to reflections from the anisotropic large-scale surface. The ϕ dependence decreases with decreasing wind speed, and the 3 m/s curve is essentially flat. In contrast, the anisotropy shown by the measurements does not change much with wind speed, and at low wind speeds it is probably due to a directional small-scale spectrum.

Parametric computations for 14.6 GHz are presented in Figures 6 through 11. The upwind-crosswind and upwind-downwind ratios of σ^0 are plotted versus θ in Figures 6 and 7 for horizontal and vertical polarizations. Computations for three wind speeds, 5, 10, and 20 m/s, are shown by the short-dashed, long-dashed, and solid curves, respectively. X-band measurements, which are reported in the Radar Handbook [Skolnik, 1970], are indicated by crosses and represent an average over six days during which the median wind speed was 5 m/s. The measured upwind-downwind ratio drops sharply at $\theta = 10^0$. In comparison, the model shows a dip but not as extreme because of the small skewness in the large-scale slope probability. For the larger angles the upwind-downwind ratio becomes greater than unity for both the computations and observations, although the 5 m/s curve is essentially at 0 db. The discrepancy at large angles is probably due in part to neglecting the small-scale anisotropy, which seems to be an important factor for light winds.

The average $<\sigma^0>$ of σ^0 over ϕ is plotted versus θ in Figures 8 and 9 for horizontal and vertical polarizations.

$$<\sigma^0> = \tfrac{1}{4}(\sigma^0_{up} + 2\sigma^0_{cross} + \sigma^0_{down}) \tag{42}$$

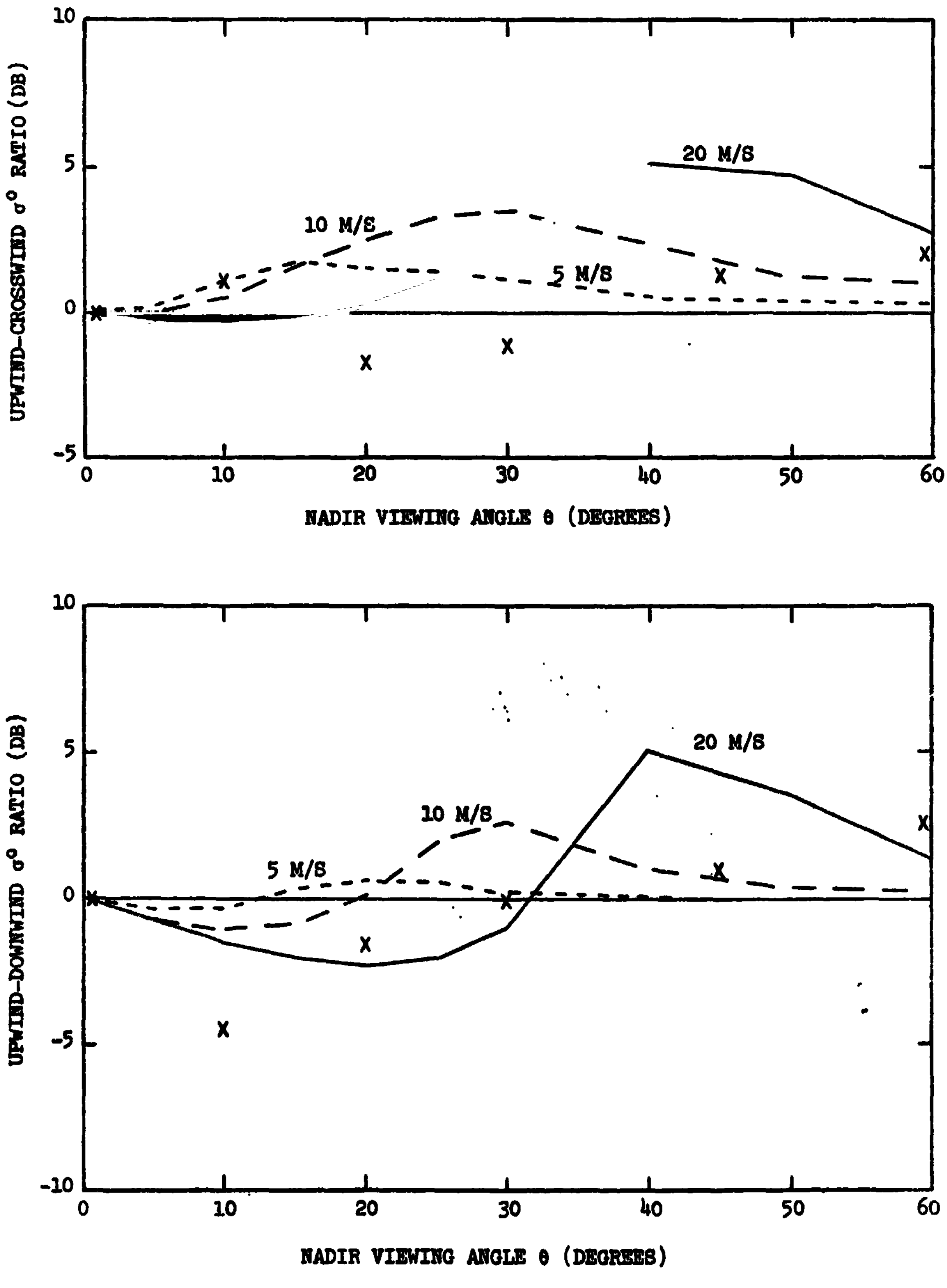

Fig. 6. Upwind-crosswind and upwind-downwind σ^0 ratios for horizontal polarization

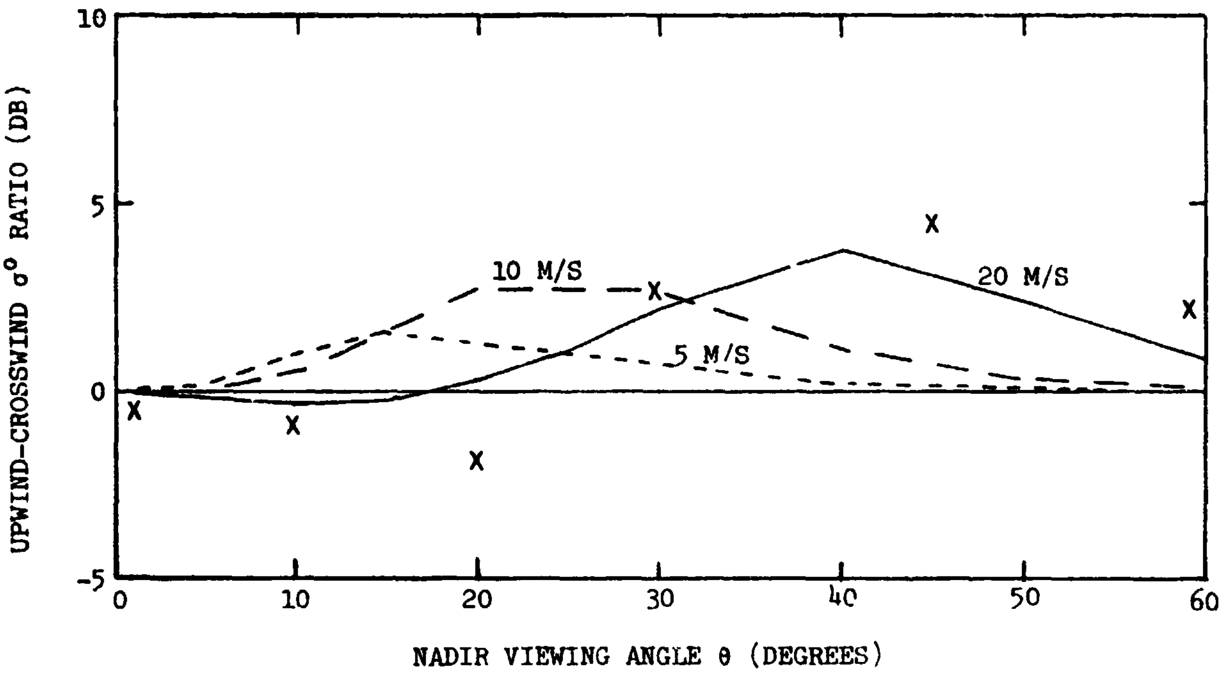

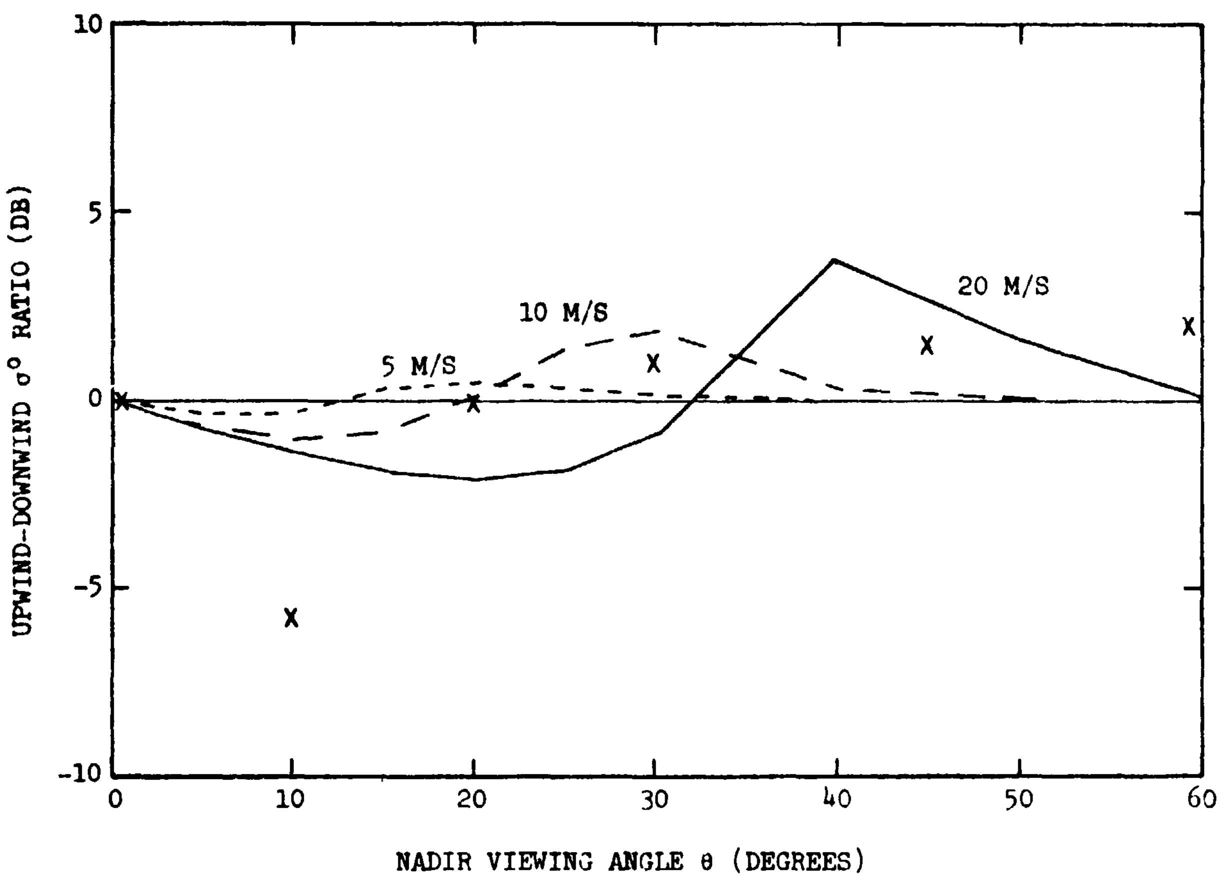

Fig. 7. Upwind-crosswind and upwind-downwind σ^0 ratios for vertical polarization

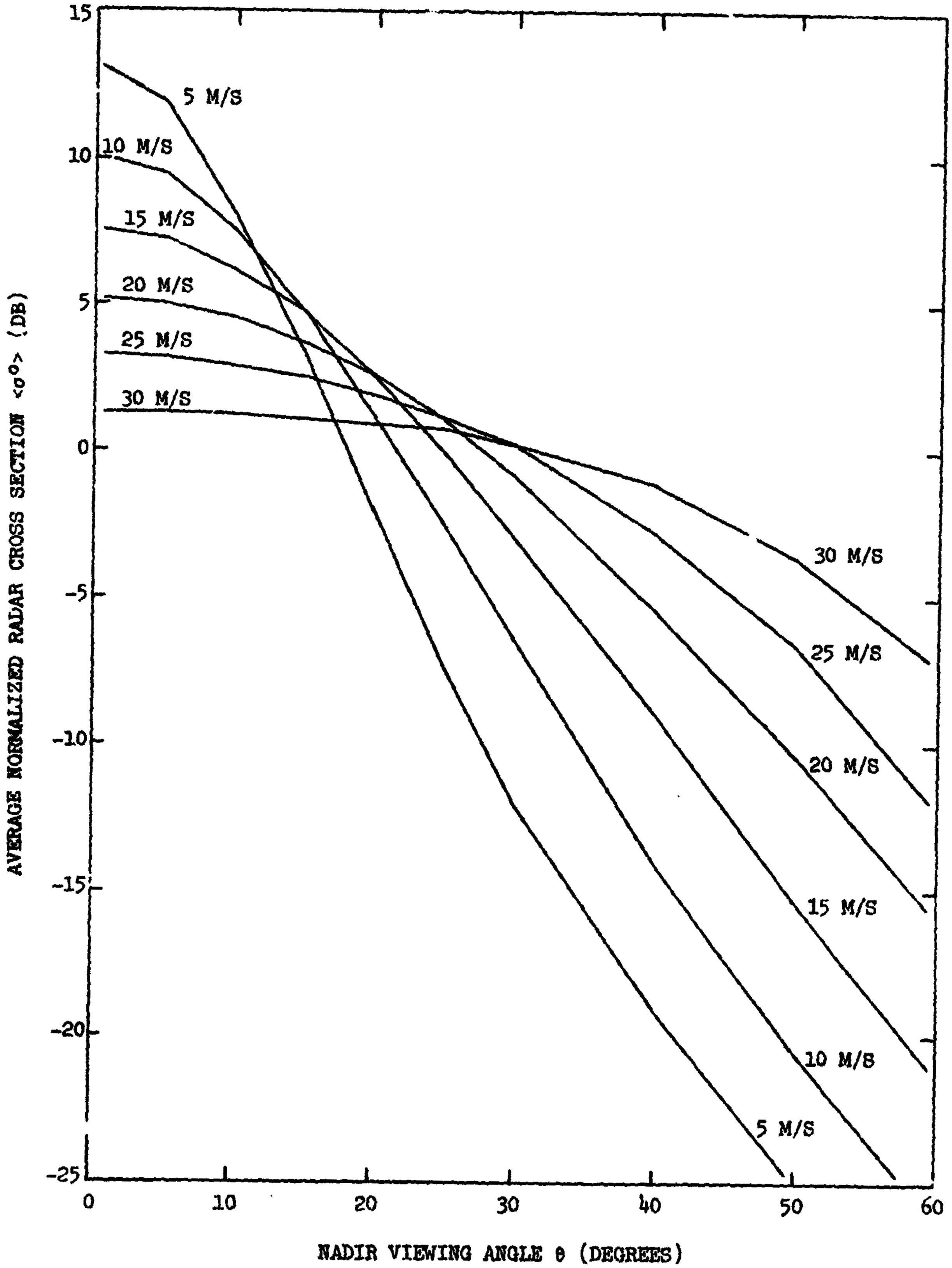

Fig. 8. The horizontally polarized $<\sigma^0>$ versus the nadir viewing angle

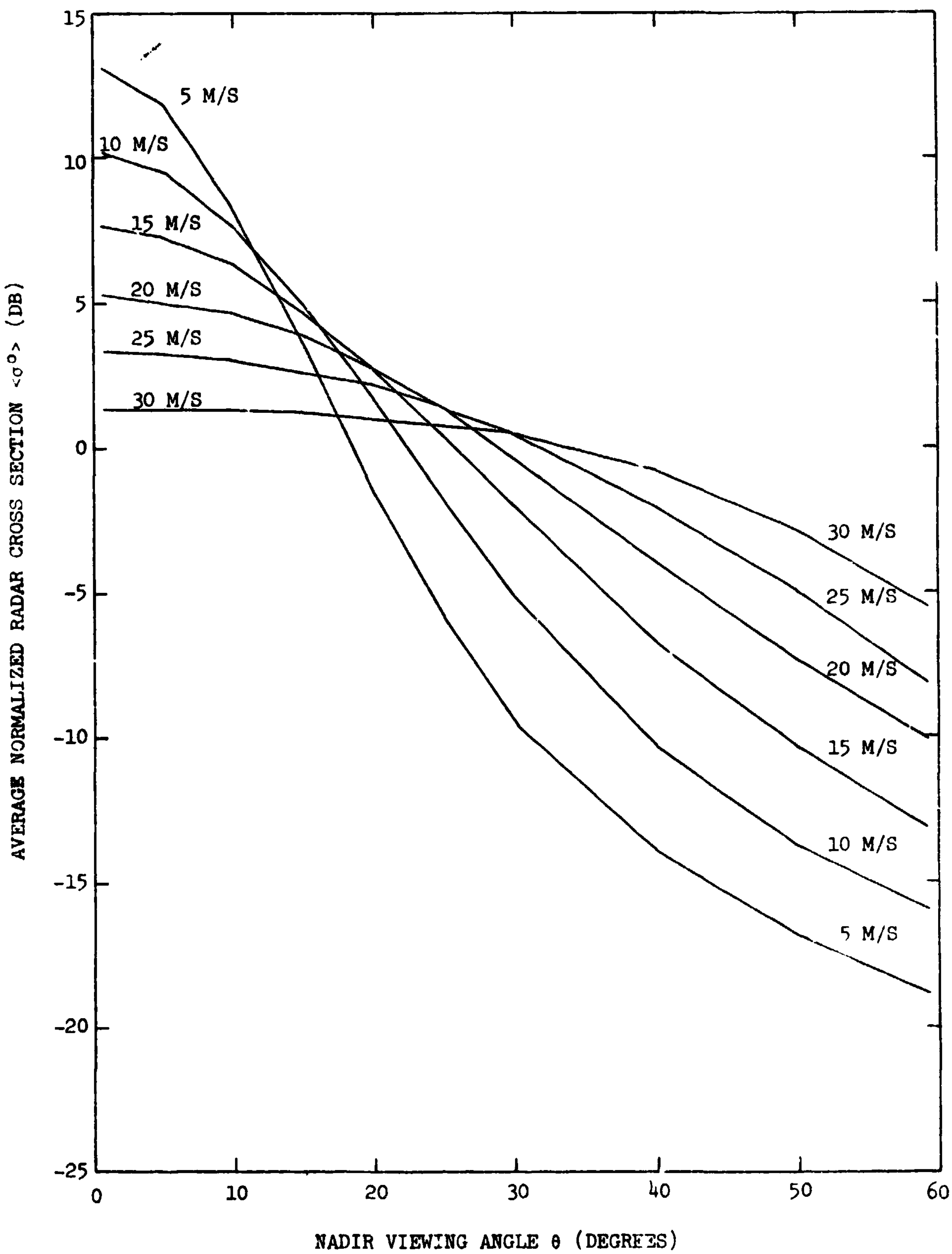

Fig. 9. The vertically polarized $<\sigma^o>$ versus the nadir viewing angle

Six wind speeds, ranging from 5 to 30 m/s in 5 m/s steps, are shown. The curves cross each other between 10° and 30°, but just considering the 5, 10, and 15 m/s curves, the crossover region is more narrow, being between 10° and 15°. The curves flatten out considerably with increasing wind speed, and $\langle\sigma^0\rangle$ at 30 m/s drops only about 8 db from 0° to 60° and is nearly independent of polarization. The polarization independence is due to the dominance of large-scale reflections for strong winds.

The same computations that appear in Figures 8 and 9 appear again in Figures 10 and 11 except that they are plotted versus the log of wind speed rather than θ. Curves for ten nadir viewing angles are shown. Near nadir $\langle\sigma^0\rangle$ decreases with increasing wind speed, and for the larger angles the opposite is true. The curve for $\theta = 15^0$ is least sensitive to wind speed variations. At the larger angles the horizontally polarized $\langle\sigma^0\rangle$ has a stronger dependence on wind speed than does the vertically polarized $\langle\sigma^0\rangle$. At 30° the wind dependence is about the same, being U^2 for horizontal polarization and $U^{1.5}$ for vertical polarization when $U \leq 20$ m/s.

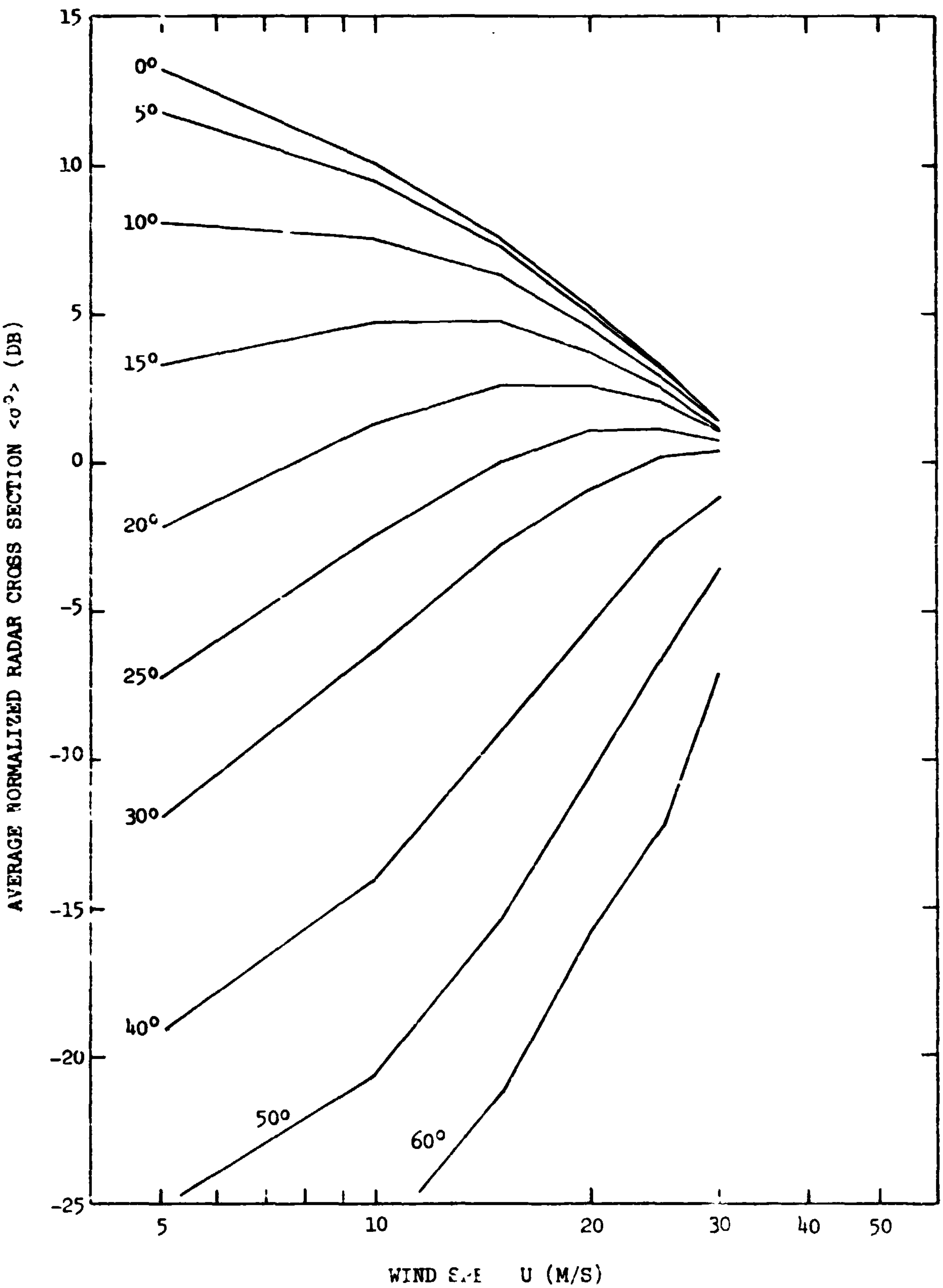

Fig. 10. The horizon'..lly polarized <σ°> ..er f the wind speed

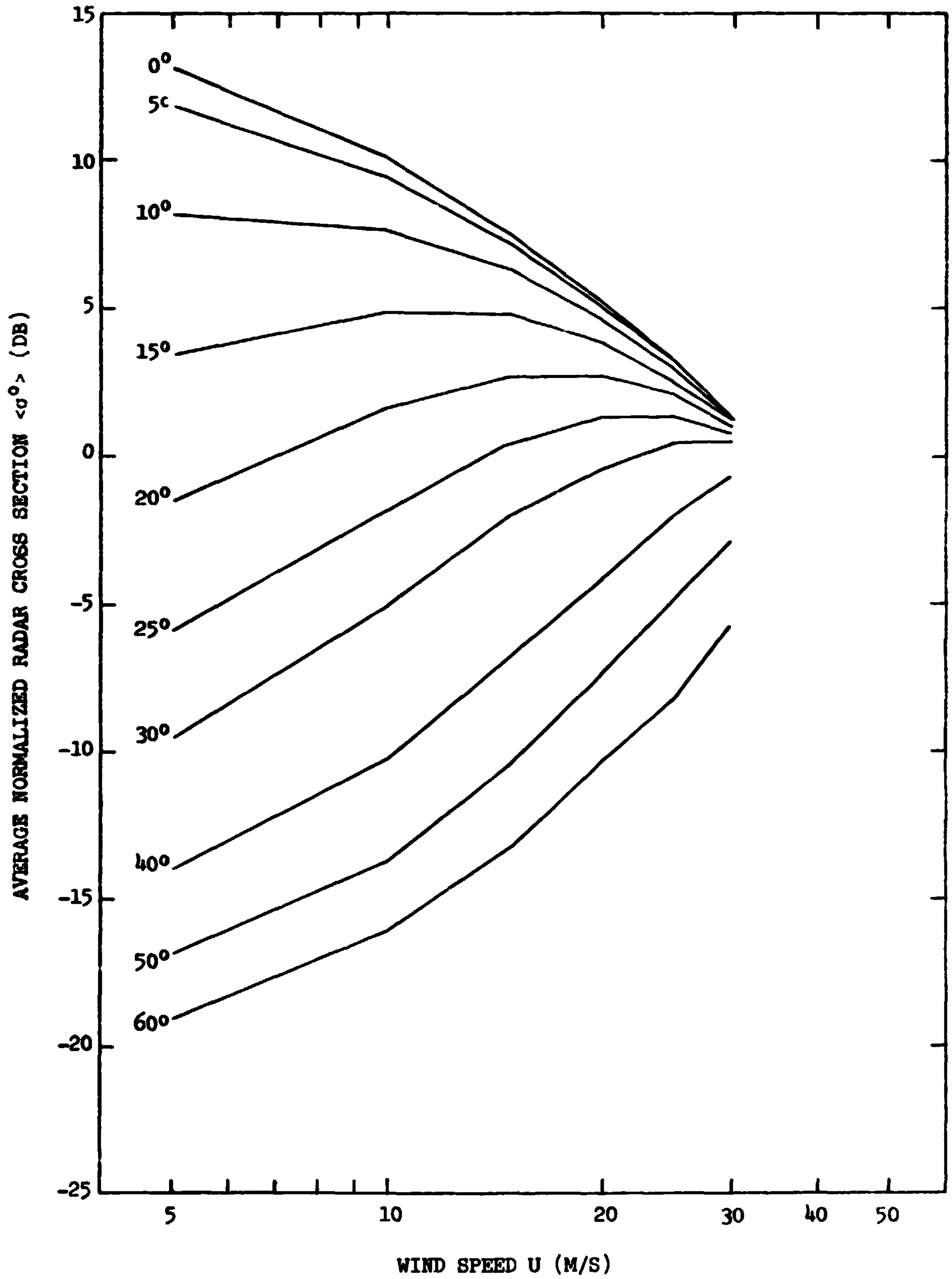

Fig. 11. The vertically polarized $<\sigma^0>$ versus the log of the wind speed

APPENDIX: SMALL-SCALE SCATTERING COEFFICIENT

According to Rice's [1951] perturbation theory, a plane wave incident onto a random, slightly rough surface Σ_s produces an incoherent scattered field and a coherent reflected field. The scattered field is represented by a set of plane waves, and the electric field $\vec{E}(\hat{k}_s)$ of one such plane wave having a propagation vector $\hat{k}_s$ is (suppressing the time dependence)

$$\vec{E}(\hat{k}_s) = [(\hat{P}_i\cdot\hat{H}_i)(\beta_{hh}\hat{H}_s + \beta_{hv}\hat{V}_s) + (\hat{P}_i\cdot\hat{V}_i)(\beta_{vh}\hat{H}_s + \beta_{vv}\hat{V}_s)]\exp[ik(\hat{k}_s\cdot\vec{r})] \quad \text{(A1)}$$

where k is the radiation wavenumber, $\vec{r}$ is the position vector, and $\hat{P}_i$ is the polarization vector of the incident field. The incident horizontal and vertical polarization vectors, $\hat{H}_i$ and $\hat{V}_i$, that are referenced to the normal $\hat{n}$ to the mean surface are given by

$$\hat{H}_i = \hat{k}_i\times\hat{n}/|\hat{k}_i\times\hat{n}| \quad \text{(A2)}$$

$$\hat{V}_i = \hat{k}_i\times\hat{H}_i \quad \text{(A3)}$$

where $\hat{k}_i$ is the propagation vector of the incident plane wave. The scattered polarization vectors, $\hat{H}_s$ and $\hat{V}_s$, are given by (A2) and (A3) with the subscript s replacing the subscript i. Peake and Barrick [1967] derived the scattering terms β_{mn}, m = h or v and n = h or v, to first order in the perturbation parameter $k\zeta$, where ζ equals the rms surface height variance.

$$\beta_{mn} = -2k(-\hat{k}_i\cdot\hat{n})\alpha_{mn}N(\vec{\kappa}) \quad \text{(A4)}$$

where $N(\vec{\kappa})$ is the coefficient of the roughness spectral component having the vector wavenumber $\vec{\kappa}$.

$$\vec{\kappa} = k\{(\hat{k}_s-\hat{k}_i) - [(\hat{k}_s-\hat{k}_i)\cdot\hat{n}]\hat{n}\} \quad \text{(A5)}$$

The bistatic matrix elements α_{mn} are given by Peake and Barrick in terms of the surface permittivity ϵ and the angles θ_i, θ_s, and Φ_s. These angles are related to $\hat{k}_i$, $\hat{k}_s$, and $\hat{n}$ by the following equations:

$$\theta_i = \arccos(-\hat{k}_i \cdot \hat{n}) \tag{A6}$$

$$\theta_s = \arccos(\hat{k}_s \cdot \hat{n}) \tag{A7}$$

$$\Phi_s = \arccos(\hat{H}_i \cdot \hat{H}_s) \tag{A8}$$

We use the convention that the first α subscript refers to the incident polarization and the second subscript refers to the scattered polarization. Peake and Barrick used the opposite convention. Also our $\hat{H}_s$ is the negative of that defined by them. Accordingly the following are the appropriate substitutions:

$$\alpha_{hh} = -\alpha'_{hh} \tag{A9}$$

$$\alpha_{hv} = \alpha'_{vh} \tag{A10}$$

$$\alpha_{vh} = -\alpha'_{hv} \tag{A11}$$

$$\alpha_{vv} = \alpha'_{vv} \tag{A12}$$

where the α'_{mn} are those appearing in Peake and Barrick [1967].

Let $\hat{P}_s$ denote the polarization vector of the receiver. The $\hat{P}_s$ polarization component of the time-averaged power of plane wave $\hat{k}_s$ divided by the time-averaged incident power is given by (* denotes complex conjugate)

$$\gamma(\hat{k}_i,\hat{k}_s,\hat{n}) = \left\langle \left| \vec{E}(\hat{k}_s) \cdot \hat{P}_s^* \right|^2 \right\rangle (\hat{k}_s \cdot \hat{n}) / (-\hat{k}_i \cdot \hat{n}) \tag{A13}$$

where the angle brackets denote average over time. The surface roughness is assumed to experience random flucuations in time such that the time-averaged electric fields of the scattered plane waves are uncorrelated, and as a result the powers of the individual scattered plane waves are additive. The assumption of random roughness also implies

$$\langle |N(\vec{\kappa})|^2 \rangle = \tfrac{1}{4}\, \kappa_0^2\, W(\vec{\kappa}) \tag{A14}$$

where $W(\vec{\kappa})$ is the roughness spectrum defined by Rice and κ_0 is the wavenumber of the fundamental roughness spectral component.

The assumption that k is much larger than κ_0 is made, and as a result the scattered waves are close together in $\hat{k}_s$-space, with the spacing being

$$\Delta k_s^x \, \Delta k_s^y = (\kappa_0/k)^2 \, k_s^z/(\hat{k}_s \cdot \hat{n}) \tag{A15}$$

The $\hat{k}_s$-space distribution of scattered power is approximated by a continuous distribution for which the power of the discrete plane waves is evenly spread over the spacings given by (A15). The scattering coefficient for the incoherent power is then given by

$$\Gamma_x(\hat{k}_i,\hat{k}_s,\hat{n}) = \gamma(\hat{k}_i,\hat{k}_s,\hat{n})/\Delta k_s^x \, \Delta k_s^y \tag{A16}$$

Combining the above equations yields

$$\Gamma_x(\hat{k}_i,\hat{k}_s,\hat{n}) = k^4(-\hat{k}_i\cdot\hat{n})(\hat{k}_s\cdot\hat{n})^2 \, W(\vec{\kappa}) \; |T|^2/k_s^z \tag{A17}$$

$$T = (\hat{P}_i\cdot\hat{H}_i)[(\hat{P}_s^*\cdot\hat{H}_s)\alpha_{hh} + (\hat{P}_s^*\cdot\hat{V}_s)\alpha_{hv}] + (\hat{P}_i\cdot\hat{V}_i)[(\hat{P}_s^*\cdot\hat{H}_s)\alpha_{vh} + (\hat{P}_s^*\cdot\hat{V}_s)\alpha_{vv}] \tag{A18}$$

The coherent reflected field is represented by a single plane wave propagating in the specular direction $\hat{k}_r$.

$$\hat{k}_r = \hat{k}_i + 2(-\hat{k}_i\cdot\hat{n})\hat{n} \tag{A19}$$

The reflected electric field is given by

$$\vec{E}(\hat{k}_r) = [(\hat{P}_i\cdot\hat{H}_i)R_h \, \hat{H}_r + (\hat{P}_i\cdot\hat{V}_i)R_v \, \hat{V}_r]\exp[ik(\hat{k}_r\cdot\vec{r})] \tag{A20}$$

where the reflected horizontal and vertical polarization vectors, $\hat{H}_r$ and $\hat{V}_r$, are given by (A2) and (A3) with the subscript r replacing the subscript i. Wu and Fung [1972] expressed the horizontal and vertical polarization reflection coefficients, R_h and R_v, in the form

$$R_m = \rho_m(\theta_i)\ (1 - Q_m) \tag{A21}$$

$$Q_m = (k \cos \theta_i/2) \int_{-\infty}^{\infty} du \int_{-\infty}^{\infty} dw\ W(\vec{\kappa})\ F_m(u,w) \tag{A22}$$

where m = h or v, $\rho_m(\theta_i)$ are the Fresnel reflection coefficients, and the functions $F_m(u,w)$ are given by Wu and Fung and have an implicit dependence on the surface permittivity ϵ, k, and θ_i. The roughness vector wavenumber $\vec{\kappa}$ in this case is given by the two-dimensional vector

$$\vec{\kappa} = (u - k \sin \theta_i\ ,\ w) \tag{A23}$$

Note that Q_m is of order $(k\zeta)^2$.

The $\hat{P}_s$ polarization component of the time-averaged reflected power divided by the time-averaged incident power is

$$\gamma(\hat{k}_i,\hat{n}) = |\vec{E}(\hat{k}_r)\cdot\hat{P}_s^*|^2 \tag{A24}$$

The scattering coefficient for the coherent power equals zero for all $\hat{k}_s \neq \hat{k}_r$, and its integral over all $\hat{k}_s$ equals $\gamma(\hat{k}_i,\hat{n})$. It thus has the form

$$\Gamma_o(\hat{k}_i,\hat{k}_s,\hat{n}) = \gamma(\hat{k}_i,\hat{n})\ \delta(k_s^x - k_r^x)\ \delta(k_s^y - k_r^y) \tag{A25}$$

where δ denotes the Dirac delta function. The total scattering coefficient for the random, slightly rough surface Σ_s is then

$$\Gamma(\hat{k}_i,\hat{k}_s,\hat{n}) = \Gamma_x(\hat{k}_i,\hat{k}_s,\hat{n}) + \Gamma_o(\hat{k}_i,\hat{k}_s,\hat{n}) \tag{A26}$$

We now consider the special case of backscattering, i.e., $\hat{k}_s = -\hat{k}_i$. The bistatic matrix elements for backscattering are

$$\alpha_{hh} = (1 - \varepsilon)/[\cos\theta_i + (\varepsilon - \sin^2\theta_i)^{\frac{1}{2}}]^2 \tag{A27}$$

$$\alpha_{hv} = 0 \tag{A28}$$

$$\alpha_{vh} = 0 \tag{A29}$$

$$\alpha_{vv} = (\varepsilon - 1)[(\varepsilon - 1)\sin^2\theta_i + \varepsilon]/[\varepsilon\cos\theta_i + (\varepsilon - \sin^2\theta_i)^{\frac{1}{2}}]^2 \tag{A30}$$

We also require that the transmitted polarization equals the received polarization, i.e., $\hat{P}_i = \hat{P}_s$, and that the roughness spectrum $W(\vec{\kappa})$ be isotropic and depends only on $|\vec{\kappa}|$. Under these conditions the incoherent backscattering coefficient becomes

$$\Gamma_x(\hat{k}_i,-\hat{k}_i,\hat{n}) = k^4\cos^3\theta_i\, W(2k\sin\theta_i)\,\big|\,|\hat{P}_i\cdot\hat{H}_i|^2\alpha_{hh} - |\hat{P}_i\cdot\hat{V}_i|^2\alpha_{vv}\big|^2/(-k_i^z) \tag{A31}$$

The scattering coefficients are integrated over $\hat{n}$ to obtain the two-scale scattering coefficients. The two-scale coherent backscattering coefficient contains the term $\gamma(\hat{k}_i,-\hat{k}_i)$. Under the above stated conditions (A24) takes the following form when $-\hat{k}_i$ is substituted for $\hat{n}$:

$$\gamma(\hat{k}_i,-\hat{k}_i) = |\rho(0)|^2\,(1 - 2\,\mathrm{Re}\,Q) \tag{A32}$$

$$Q = (\pi k/2)\int_0^\infty du\, u\, W(u)\,\left[2k\varepsilon^{\frac{1}{2}} + 2b - 2c + u^2(c - b)(u^2 + bc)^{-1}\right] \tag{A33}$$

$$b = (k^2 - u^2)^{\frac{1}{2}} \tag{A34}$$

$$c = (\varepsilon k^2 - u^2)^{\frac{1}{2}} \tag{A35}$$

where b is either positive real or negative imaginary. The Fresnel reflection coefficient for normal incidence is

$$\rho(0) = (1 - \epsilon^{\frac{1}{2}})/(1 + \epsilon^{\frac{1}{2}}) \tag{A36}$$

where in this case the sign is arbitrary. Note that in (A32) the $|Q|^2$ term, which is of order $(k\zeta)^4$, has been dropped.

Wentz [1974] proves that the above formulation satisfies energy conservation to second order in $k\zeta$. The proof entails taking the sum of the scattering coefficients given by (A26) for two orthogonal scattered polarizations. The integral of this sum over all $\hat{k}_s$ is then shown to equal unity for a perfect conductor.

REFERENCES

Cardone, V. J., Specification of the wind field distribution in the marine boundary layer for wave forecasting, Rep. TR 69-1, Geophys. Sci. Lab., New York Univ., New York, Dec. 1969.

Cox, C., and W. Munk, Slopes of the sea surface deduced from photographs of sun glitter, Bul. Scripps Inst. Oceanog. 6, 401-488, 1956.

Peake, W. H., Interaction of electromagnetic waves with some natural surfaces, IRE Trans. Antennas Propagat., 7, Special Suppl., S324-S329, 1959.

Peake, W. H., and D. E. Barrick, Scattering from surfaces with different roughness scales: Analysis and interpretation, Res. Rep. BAT-197A-10-3, Battelle Mem. Inst., Columbus, Ohio, Nov. 1967.

Pierson, W. J., and R. A. Stacy, The elevation, slope, and curvature spectra of a wind roughened sea surface, Contract. Rep. NASA CR-2247, Langley Research Center, Hampton, VA, Dec. 1973.

Porter, R. A., and F. J. Wentz, Microwave radiometric study of ocean surface characteristics, Contract. Rep. 1-35140, Nat. Environ. Satell. Serv., NOAA, Washington, D. C., July 1971.

Rice, S. O., Reflection of electromagnetic waves from slightly rough surfaces, Commun. Pure Appl. Math., 4, 351-378, 1951.

Skolnik, M. I., ed., Radar Handbook, chapter 26, McGraw Hill, New York, 1970.

Wentz, F. J., The effect of surface roughness on microwave sea brightness temperatures, Contract. Rep. 3-35345, Nat. Environ. Satell. Serv., NOAA, Washington, D. C., March 1974.

Wentz, F. J., Cox and Munk's sea surface slope variance, J. Geophys. Res. 81 (9), 1607-1608, March 1976.

Wu, S. T., and A. K. Fung, A noncoherent model for microwave emissions and backscattering from the sea surface, J. Geophys. Res. 77(30), 5917-5929, 1972.

1. Report No.	2. Government Accession No.	3. Recipient's Catalog No.
NASA CR-145278		
4. Title and Subtitle: Radar Backscattering from a Sea Having an Anisotropic Large-Scale Surface		5. Report Date: November 1977
		6. Performing Organization Code
7. Author(s): Frank J. Wentz		8. Performing Organization Report No: Part II
		10. Work Unit No.
9. Performing Organization Name and Address: Frank J. Wentz and Associates, Box 162, MIT Branch P.O., Cambridge, MA 02139		11. Contract or Grant No: L-24420A
		13. Type of Report and Period Covered: Final Report
12. Sponsoring Agency Name and Address: National Aeronautics and Space Administration, Washington, D.C. 20546		14. Sponsoring Agency Code
15. Supplementary Notes		

16. Abstract

The scattering of radiation from a rough sea is modeled by combining geometric optics and small-scale perturbation theory in a manner consistent with energy conservation. The sea surface is represented by an isotropic small-scale surface superimposed onto an anisotropic large-scale surface. The special case of backscattering for like polarizations is considered, and computations of the normalized radar cross section $\sigma°$ are compared with the AAFE RADSCAT data at 13.9 GHz. Computations of $\sigma°$ at 14.6 GHz are also presented, and the dependence of $\sigma°$ on the nadir and azimuth viewing angles and on the wind speed is analyzed.

17. Key Words (Suggested by Author(s))	18. Distribution Statement
Microwave backscatter Sea-surface two scale roughness Scattering measurements at 13.9 GHz	Unclassified Unlimited — Subject Category 48

19. Security Classif. (of this report)	20. Security Classif. (of this page)	21. No. of Pages	22. Price*
Unclassified	Unclassified	34	$4.50

* For sale by the National Technical Information Service, Springfield, Virginia 22161